Publicado en 2018, Fuel, 233, pp. 851-859

In-Situ Generation of CO_x-Free H_2 by Catalytic Ammonia Decomposition over Ru-Al-Monoliths.

Sabino Armenise[a,b,c *], Fernando Cazaña[b], Antonio Monzón[b], Enrique García-Bordejé[c]

[a] Universidad Politécnica Salesiana, Department of Biotechnology, Av. 12 Octubre, 170109, Quito, Ecuador.

[b] Institute of Nanoscience of Aragon. Department of Chemical and Environmental Engineering. University of Zaragoza. 50018, Zaragoza. Spain

[c] Instituto de Carboquímica (ICB-CSIC), Miguel Luesma Castán 4, 50018 Zaragoza, Spain.

Abstract

Ru catalysts supported on alumina coated monoliths has been prepared employing three different precursor, which are ruthenium chloride, ruthenium nitrosyl nitrate and ruthenium acetyl acetonate, by an equilibrium adsorption method. The Ru particle sizes could be controlled varying the metal precursor salt. Among the prepared catalysts, Ru catalyst prepared from nytrosyl nitrate exhibited the highest activity which is concomitant to the largest mean Ru particle size of 3.5 nm. The values of the apparent activation energy calculated from the Arrhenius equation are accoding to the Temkin-Phyzev model, indicating that the recombinative desorption of N ad-atoms is the rate-determining step of the reaction. However, the ratio between the kinetic orders with respect to ammonia and hydrogen ($-\alpha/\beta$), is not in agreement to the valued predict by Temkin formalism. This fact could be related to the different operational conditions used during the reaction, and/or catalyst nature, but not to any change on the controlling step of the reaction.

Keywords: Structured Reactors; Ru-Catalyst; Ammonia Decomposition; Kinetics; COx-Free; Nanoparticle.

* Corresponding author. Tel.:+ 593 994787533; Email: sarmenise@ups.edu.ec

1. Introduction

Hydrogen combined with PEM fuel cells have attracted great interest recently as substitute of fossil fuels in locomotion and other fields. However, hydrogen storage and transportation involves great technical challenges to overcome. Its low energy per volume unit, along with its flammability are factors which make difficult its storage as gas at normal pressure [1]. Because of that, several technologies for hydrogen storage have been proposed. These include storage at high pressures, either in liquid form or adsorbed in a solid [2,3]. However, liquid H_2 requires high energy consumption and expensive leak-free tanks. A more interesting option is the chemical storage in form of easily storable and with high hydrogen content compounds, such as light hydrocarbons or ammonia. These compounds must be decomposed in-situ to release a hydrogen stream to feed the fuel cell. Recently, the production of hydrogen from the decomposition of light hydrocarbons as methane, ethane or ethanol has attracted a great researching interest [4]. Nevertheless, all these processes have the inherent drawback of producing CO_x along with the H_2 stream. CO_x acts as poisons for PEM fuel cells, even at concentrations as low as a few ppm [5]. Therefore, systems based on hydrocarbons decomposition must include a series of purification steps, like desulfurization, water gas shift, methanation, and preferential oxidation to reduce CO_x levels in the reformer outlet gas. Ammonia, on the other hand, produces a CO_x-free stream of hydrogen, and unconverted ammonia can be easily reduced to safe levels in one-step adsorption. In addition, ammonia has a high H_2 content (17.7% wt) and can be stored in liquid form at mild conditions (room temperature and 6 atms). For the whole process of H_2 storage as NH_3 to be environmentally sustainable, the H_2 and the energy required for synthesis and decomposition process should be produced using renewable energies. On the other hand, the energy needed for decomposition of NH_3 could be generated using a small

54 percentage of the energy stored in NH_3. This percentage will be minimized if a catalyst
55 active at the lowest temperature as possible is used and obtaining a high-purity H_2
56 stream. All this characteristic make more economically feasible the hydrogen
57 production from ammonia than others career [6].
58 In the last years, ammonia decomposition reaction has been extensively studied for H_2
59 generation, including the catalytic active phase to the reactor structure and design [7].
60 Yin et al., reported that ruthenium exhibits the highest TOF in ammonia decomposition
61 [8]. Therefore, research has been focused on ruthenium supported on different carriers,
62 such as alumina [9–11] or others transition metal oxides like MgO [12], activated
63 carbon [13,14], or carbon nanotubes/nanofibers [15–18]. Bimetallic combinations of
64 transition metals (MoCo) have also proved to be active enough to replace ruthenium
65 catalyst [19–23]. From the point of view of reactor design, microestructured reactors
66 have improved the performance of the conventional packed bed reactors [24–27].
67 One century after the development of Habber-Bosch process, ammonia mechanism still
68 being investigated by several authors to obtain more precise information about reaction
69 mechanism and to explain the wide range differences observed on the kinetic
70 parameters.
71 The mechanism of ammonia decomposition reaction has been grouped in two limiting
72 cases: (i) effect of ammonia concentration, (ii) effect of hydrogen concentration.
73 At low ammonia concentrations and low temperatures [28,29], the reaction rate shows
74 non-dependence with respect to ammonia. However, at high temperatures the reaction
75 becomes first-order with respect to ammonia [30,31]. These transition temperature has
76 been investigated by Tamaru [32] and Chellappa [33], and explained by a change of
77 reaction mechanism. At temperature below 650 K the recombinative desorption of N-

adsorbed species is the rate-determining step (RDS), while at high temperature (< 750 K), cleavage of N-H bond on NH_3 adsorbed species is the RDS [30,31].

At high hydrogen partial pressure and low temperature, the reaction is found to be inhibited by hydrogen [33]. In these operational conditions the reaction is explained by Temkin-Phyzev mechanism [32,34]. This reaction mechanism assumes that both recombinative desorption of N-species and N-H cleavage are the RDS. Inhibitory effects of hydrogen could be associated to the re-hydrogenation of N-species adsorbed or by blocking the active sites by competitive adsorption, where ammonia decomposition takes place. At high temperature and low hydrogen partial pressure (low conversion), Temkin-Phyzev model could be re-written as Tamaru`s model [32,35].

This work is a new contribution of our group to the study of the ammonia decomposition reaction, using nickel catalysts supported on honeycomb monoliths prepared by electrostatic adsorption structured reactors [27]. Herein, our aim is to investigate the performance of Ru-based reactors, and in particular, to obtain uniformly dispersed Ru nanoparticles in alumina coated monoliths. To this end, different Ru precursors were tested. The catalysts after reduction were characterized by STEM, TPR and XPS and tested in the decomposition of pure ammonia. Also a kinetic study is carried out in other to determine the effect of precursor synthesis on the main apparent kinetic parameters: activation energy and reaction orders.

2. Experimental

2.1. Materials and Catalyst Preparation

Cordierite monoliths were carved out from blocks supplied by Corning (400 cpsi) to the desired dimensions (65 mm long, 10 mm diameter, ca. 2,4 g). These monoliths were impregnated with alumina by a dip coating method, as described elsewhere [27]. A sol-gel was prepared by mixing pseudobohemite (AlOOH pural, from Sasol), 0.3 M nitric

acid and urea, in 2:5:1 proportion. After stirring for 24h, monoliths were immersed in the mixture until ensuring the absence of air bubbles in the channels. Following up, the excess of liquid was removed with pressurized air and the monoliths were dried for 24 hours at room temperature while rotating around its axis. Later, the monoliths were calcined under 100 ml/min air flow for 2 hours at 873 K, at a heating rate of 1 K/min.

The deposition of ruthenium nanoparticles was carried out by equilibrium adsorption or electrostatic adsorption method [36]. In this method, the ions of precursor in solution are bound by electrostatic forces to the sites of opposite charge at support surface. Three different Ru precursors were used. Ruthenium Chloride ($RuCl_3 \cdot xH_2O$) dissolved in 10 ml of 0.1M HCl, ruthenium nitrosyl nitrate ($Ru(NO_3)_3(NO)$) dissolved in 10 ml of distilled water and ruthenium acetyl acetonate ($RuC_{15}H_{21}O_6$) dissolved in 10 ml of toluene. The weight or ruthenium in solution was calculated on the basis of a nominal weight percentage of 5 wt% with respect to alumina coating. The alumina coated monoliths were fitted to a vial with the impregnating solution and rotated continuously perpendicular to its axis during 24 hours. In this process, the liquid with the precursor flows through the monoliths channels and it is concomitantly homogenized due to the rotating movement. After this process, the liquid inside the channels was removed with pressurized air and the monoliths were dried under rotation during 24 hours. Finally, they were calcined in 100 ml/min of N_2 at 873 K during 2 h, using a heating rate of 1 K/min. The monolith samples were denoted as Ru(Cl)/Al/M, Ru(NN)/Al/M and Ru(acac)/Al/M for catalysts prepared from ruthenium chloride, ruthenium nitrosyl nitrate and ruthenium acetyl acetonate, respectively. The actual Ru content was analyzed by inductive coupled plasma optical emission spectroscopy (ICP-OES) after digestion of the samples in lithium borohydride. In addition, Ni catalyst was also

prepared from a nickel nitrate solution as described previously [23]. The actual Ni loading determined by ICP-OES was 15 wt%.

2.2. Catalytic Testing

Catalyst reactivity system consists of a continuous-flow 15 mm i.d. quartz reactor inside horizontal furnace with a temperature controller (Eurotherm). The monolithic nickel catalyst was wrapped with quartz stripe and it was tightly fitted to the wall of the quartz reactor to avoid channeling. Subsequently, the reactor was placed in the constant temperature zone of the furnace. The reaction testing was carried out after catalyst reduction in hydrogen atmosphere (100 ml/min H_2:N_2, 50:50) at 773 K for 1 h. Catalysts were tested between 573 and 973 K using 100 ml/min of pure anhydrous ammonia as feed gas. The outlet reaction gases were analyzed with an Agilent Micro GC 3000A. H_2 an N_2 were analyzed in a molsieve column and ammonia in a Plot-Q column. To ensure repeatability, 2–3 separate GC samples were taken and averaged for each experimental data point, and analyses were typically within ±3% of each other. The conversion was calculated taking into account the variations in the flow due to the mole increase in the reaction.

2.3. Catalyst Characterization

The catalysts after reaction were tested by different techniques. Temperature programme reduction (TPR) was carried out in a Micromeritics AutoChem II 2920. In TPR experiments, the catalyst was heated in 50 ml/min (STP) of 10% H_2 in Ar up to 1273 K with a heating rate of 10 K/min.

XPS technique was used to measure the Ru oxidation state. The apparatus was an ESCAPlus Omnicrom system equipped with a Mg Kα radiation source to excite the

sample. Calibration of the instrument was done with Ag $3d_{5/2}$ line at 368.27eV. All measurements were performed under UHV, better than 10^{-10} Torr. Internal referencing of spectrometer energies was made using the dominating Al 2p peak of the support, at 74.0 eV and corroborated with the C 1s signal at 284.4 eV. The curve fitting of the spectra was performed using CASA XPS software after applying a Shirley baseline.

Catalyst particle size was studied by scanning transmission electron microscopy (STEM) using a FEI TECNAI F30 electron microscope equipped with Gatan Energy Filter and cold field emission gun (FEG) operated at 300 kV with 1.5 Å lattice resolution. TEM specimens were prepared by ultrasonic dispersion in ethanol of powder retrieved from the monoliths. A drop of the suspension was applied to a holey carbon support grid.

3. Results and Discussion

3.1 Textural and morphological characterization

Table 1 shows the textural properties of the prepared catalysts. All Ru catalysts exhibit similar textural properties and the surface area is comparable to that of the support (246 m^2/g). There are not significant differences between the Ru content deposited using the different salt precursors.

Table 1. Textural properties measured by N_2 physisorption and surface composition measured by XPS of Ru catalysts on alumina coated monoliths prepared from different precursors.

Catalyst	Ru/Al [1] wt%	Surface Area (m^2/g)	Pore diameter (Å)	Ru/Al[2] wt %	Ru^0/Ru_{total}[2] at.%
Ru(NN)/Al/M	3.0	238	60	6.7	69.1
Ru(Cl)/Al/M	3.6	215	60	6.4	5.7
Ru(acac)/Al/M	3.0	233	55	5.6	7.4

[1]Measured by ICP-OES

[2] Measured by XPS

The ruthenium particle size was characterized by STEM. Fig. 1 shows representative STEM images and particle size distribution (inset) for the several catalysts prepared. For Ru(NN)/Al/M (Fig. 1a, and 1b) the particles are spherical with heterogeneous distribution particle sizes, ranging between 1 and 10 nm with a mean size of 3.5 nm. On the other hand, for Ru(Cl)/Al/M and Ru(acac)/Al/M (Fig. 1c to 1f) the particle size are predominantly smaller than 1.5 nm, with a homogeneous distribution. The mean particle size is subnanometric for Ru(Cl)/Al/M and 1.5 nm for Ru(acac)/Al/M.

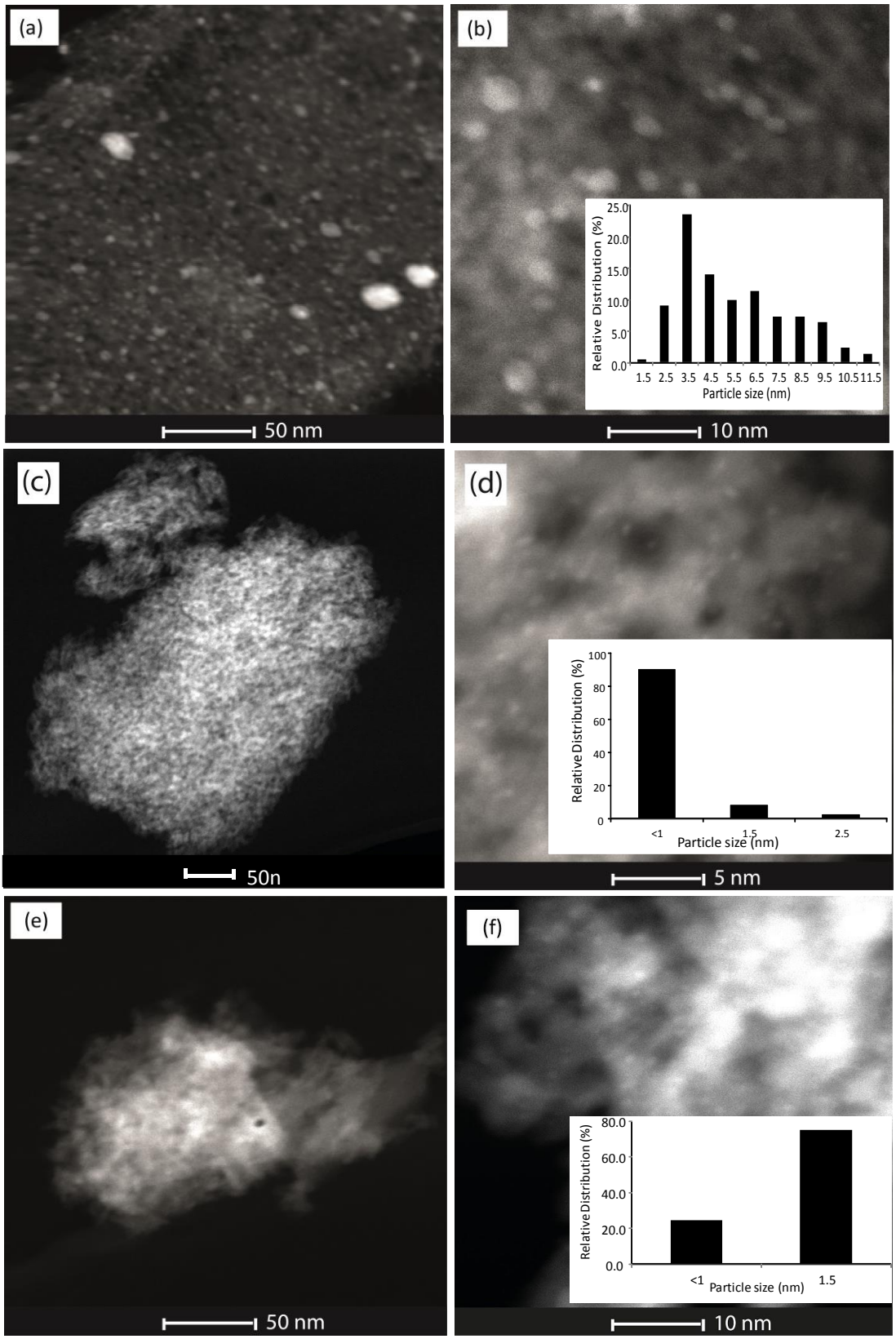

Fig. 1. Representative STEM images at two different magnifications and particle size distribution of catalysts used in reaction: (a,b) Ru(NN)/Al/M; (c,d) Ru(Cl)/Al/M y (e,f) Ru(acac)/Al/M.

3.2. Ru oxidation state characterization

Fig. 2 shows the deconvolution of XPS Ru signal according to the literature assignments [25-28]. In addition, the quantification of Ru/Al and Ru^0/Ru_{total} atomic ratios determined by XPS are displayed in table 1. The Ru/Al ratio determined by XPS is similar for all the catalysts synthesized and these ratios are around twice that those determined by ICP. This result indicates that the surface of the alumina coating is enriched by Ru.

In the deconvolution of Ru 3d XPS signal of Ru(NN)/Al/M (spectrum a of Fig. 2) only the peaks at 279.1 eV and 280.5 eV are present, which are associated to Ru^0 and RuO_2 species [37–40], respectively. However, for the catalyst Ru(Cl)/Al/M and Ru(acac)/Al/M, besides the peaks associated to Ru^0 and RuO_2, is observed a new signal centered at 282.3 eV, which can be ascribed to hydrated RuO_2 species [41]. Additionally, a peak centered at 284.4 eV has been observed in all the catalysts which is attributed to carbon contamination.

The catalysts Ru(Cl)/Al/M and Ru(acac)/Al/M show $Ru^0/Ru_{(total)}$ ratios substantially smaller than the catalyst Ru(NN)Al/M. In the XPS spectra of Ru(Cl)/Al/M, a signal at 198.5 eV was observed indicating the presence of chlorine ions. It is well known that electronegative species such as chlorine can increase the oxidation state of metals [42,43], which could explain the lower $Ru^o/Ru_{(total)}$ ratios. However, the effect of electron-withdrawing species cannot be invoked to explain the lower $Ru^0/Ru_{(total)}$ ratios of Ru(acac)/Al/M. Therefore, the most plausible explanation is that metal oxidation state is governed by interaction with the support, which is particle-size dependent. Thus, the smaller the Ru particles, the stronger is the metal support interaction, leading to lower $Ru^0/Ru_{(total)}$ ratios.

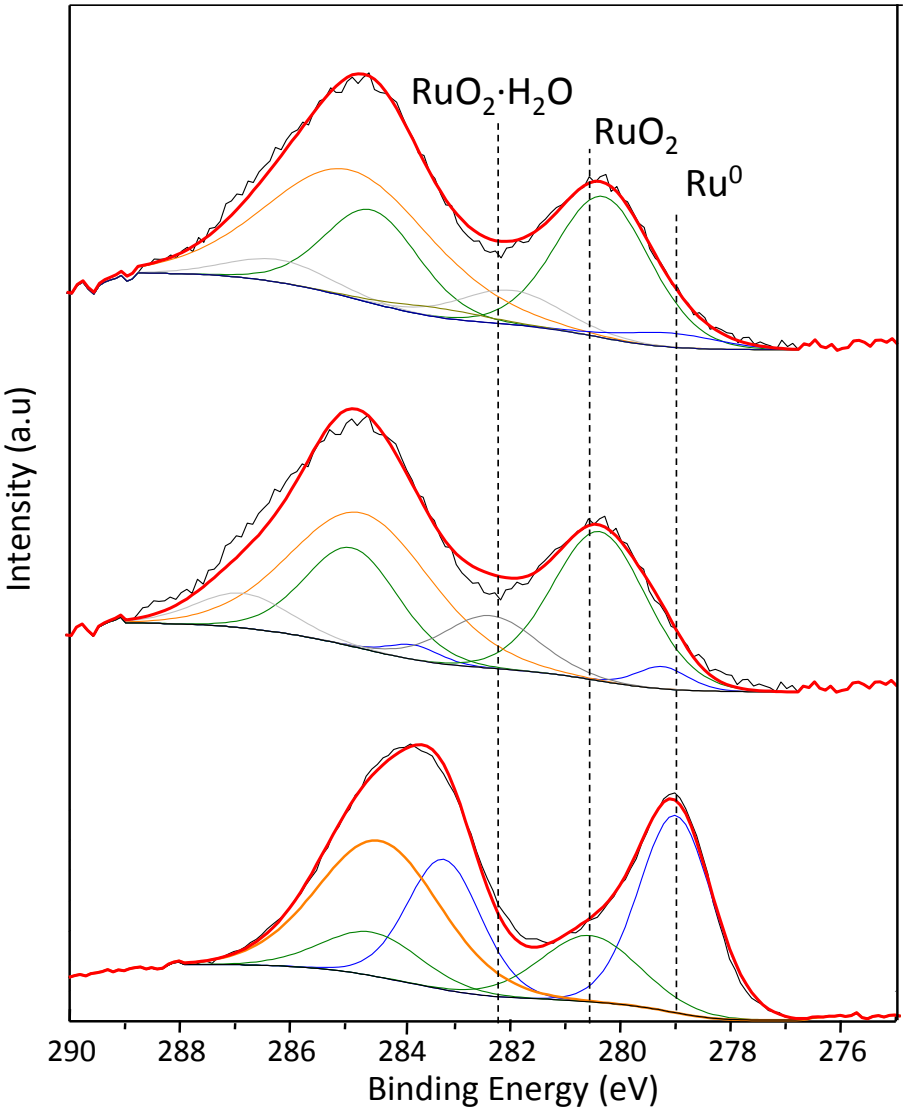

Fig. 2. XP Spectra of 3d core level of ruthenium of the catalyst used in reaction: (a) Ru(NN)/Al/M; (b) Ru(Cl)/Al/M and (c) Ru(acac)/Al/M.

The passivated catalysts after reaction were also studied by temperature programmed reduction (Fig. 3). The TPR profile of Ru(NN)/Al/M shows two peaks, one intense peak at low temperature (ca. 380 K) which can be attributed to surface oxidized large Ru nanoparticles and a broad peak at higher temperatures which can be attributed to oxidized smaller Ru particles, interacting strongly with the support. The other two catalysts, Ru(Cl)/Al/M and Ru(acac)/Al/M, exhibit similar TPR profiles with two shoulders, one at ca.430 K and other in the range of 550-750 K which correspond to RuO_2 particles with some kind of interaction with support. The peak showed at low

temperatures (380 K) is absent in these two latter catalysts, suggesting that the smaller particles, present in these catalysts, have stronger interaction with the support. On the other hand, the larger particles found for Ru(NN)/Al/M are oxidized only on the outermost surface but the inner bulk metal remains in reduced state in agreement with XPS results [21].

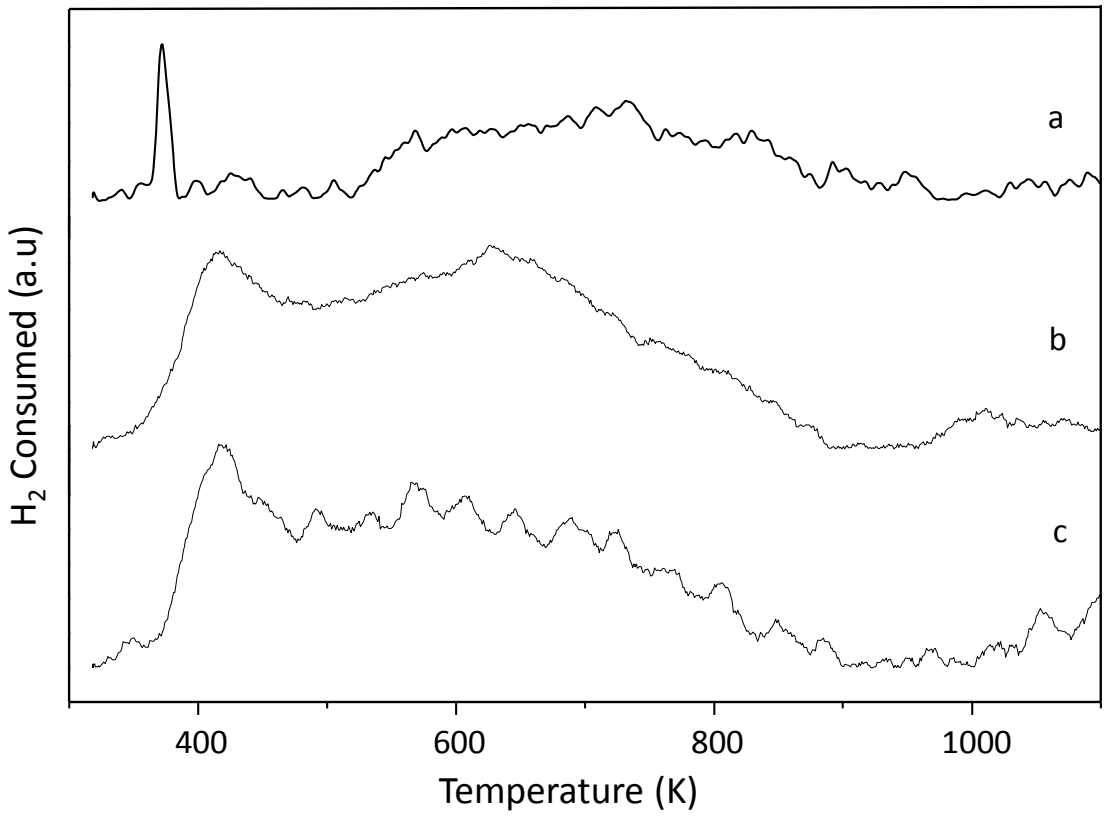

Fig. 3. TPR profile of catalysts passivated after reaction for Ru catalysts (a) Ru(NN)/Al/M; (b) Ru(Cl)/Al/M and (c) Ru(acac)/Al/M.

3.3. Catalytic testing in NH_3 decomposition

Fig. 4 shows the NH_3 conversion vs. temperature plot for the Ru-based catalysts. This Figure also includes the curve obtained for the catalyst that contains a 15% Ni on Alumina coated monolith. The preparation and characterisation of this Ni/Al/M catalyst is reported in a previous publication [44]. All Ru-based catalyst exhibit higher conversion than Ni-based catalyst although the metal loading is five-fold higher for the later, ca. 3 and 15 wt%/Al_2O_3, respectively. Noticeably, the mean particle size of Ni was

larger than for Ru catalysts, 6 nm vs. 2.5 nm for Ru(NN)/Al/M. This seems to indicate a larger intrinsic activity of Ru metal, in agreement with the literature [21].

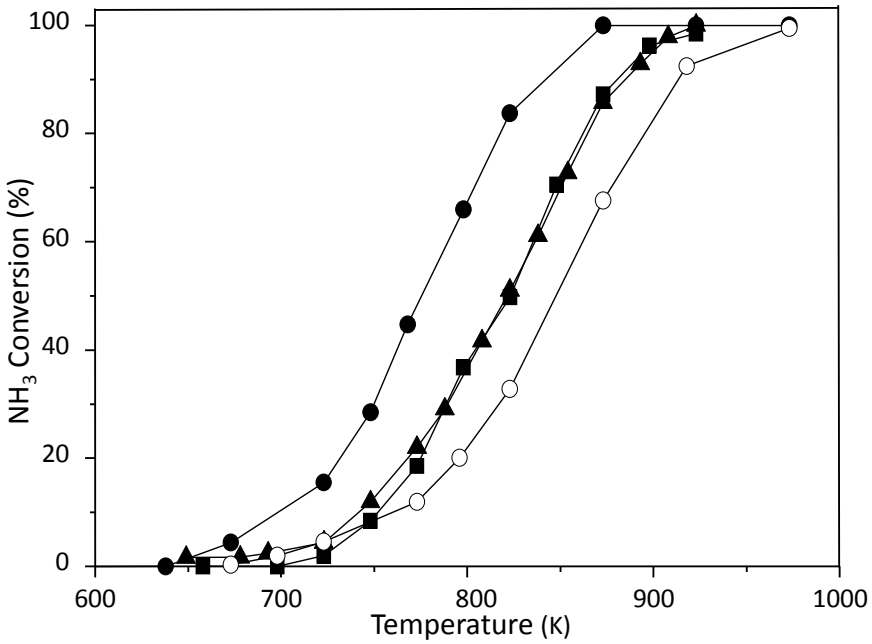

Fig. 4. NH_3 conversion at steady state as a function of the reaction temperature for different catalysts. (●) Ru(NN)/Al/M; (■) Ru(Cl)/Al/M; (▲) Ru(acac)/Al/M and (○) Ni/Al_2O_3/Monolith. Conditions: 100 ml/min pure NH_3, space velocity: 35000 h^{-1}/g Ni/Al_2O_3.

Comparing among Ru-based catalysts, the one prepared with nitrosyl nitrate (Ru(NN)/Al/M) exhibits higher conversion, for all temperatures studied, than those prepared with other precursors. Since the main difference between Ru(NN)/Al/M and the other catalysts is the particle size, it is reasonable to think that this fact may be the responsible of the different catalytic behaviour. Jacobsen and cols. reported that B_5-type sites have the adequate geometry for the ammonia decomposition [45]. The number of these sites decreases as the particle size diminishes. This fact has been experimentally confirmed by several authors, who observed an increase of the turnover frequency as the metal particle size increased [46–48]. Xu and cols. [49] reported that there was an optimum Ru particle size of 2.2 nm that maximized turnover frequency. They also found that the apparent activation energy increased from 79 kJ mol^{-1} to 122 kJ mol^{-1} as the mean Ru particle size decreased from 4.6 to 1.9 nm. The apparent activation

energies of the different catalysts prepared were calculated from the Arrhenius equation (Fig. 5) at low conversion (<10%), in order to operate into differential condition. The apparent activation energy for Ru(NN)/Al/M was 104 kJ mol^{-1}, which was smaller than those determined for Ru(acac)/Al/M and Ru(Cl)/Al/M, 120 kJ mol^{-1} and 183 kJ mol^{-1}, respectively. It is possible that presence of chorine ions may act as inhibitor in the catalyst prepared with ruthenium chloride, contributing to the lower conversion and higher apparent activation energy for this catalyst.

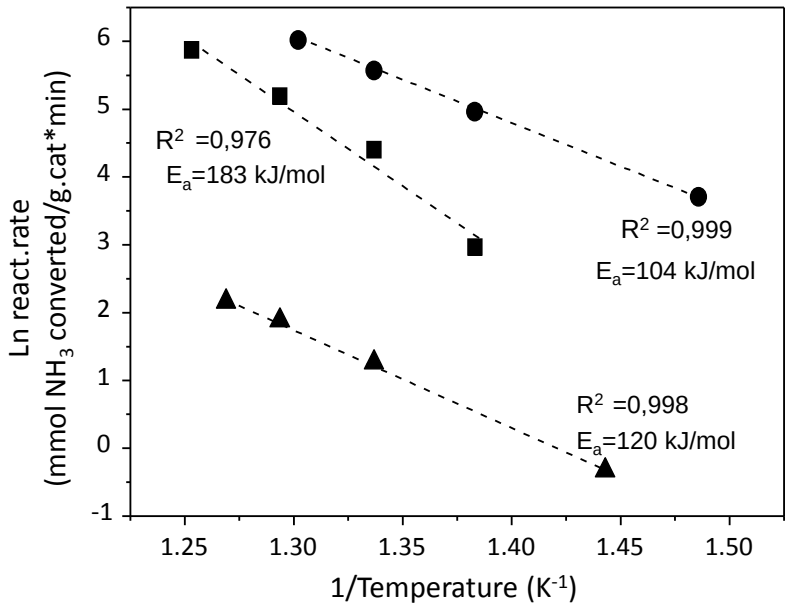

Fig. 5. Arrhenius plot and estimation of the apparent activation energies for the Ru catalysts from different precursors. (●) Ru(NN)/Al/M; (■) Ru(Cl)/Al/M; (▲) Ru(acac)/Al/M.

3.4. Kinetic Model

The development of an efficient reactor requires necessarily a depth understanding of kinetic aspects. Many researches related to ammonia decomposition reaction have been carried out under high vacuum condition and with model catalysts. These conditions are not comparable to fuel cell systems fed by ammonia decomposition reaction where usually high ammonia concentration, atmospheric pressure and high temperature have.

Regarding to ammonia decomposition kinetics, many author have fitted the experimental data using the Themkyn-Pyzhev model:

$$(-rNH_3) = k\left[\left(\frac{PNH_3{}^2}{PH_2{}^3}\right)^m - \frac{PN_2{}^2}{Keq^2}\left(\frac{PH_2{}^3}{PNH_3{}^2}\right)\right] \quad (1)$$

Where *m* is a constant related to the non-uniformity surface, and the second term corresponds to the contribution of the reversible equation (i.e. que driving force to the equilibrium). According with the experimental conditions (673 K -1023 K), and to the results previously reported [50], this term is virtually zero, indicating that the reaction is not limited by equilibrium, and therefore this contribution can be neglected.

The Temkin-Pyzhev model may be rewrite to the power law rate expression:

$$(-rNH_3) = k'\, P\mathrm{NH_3}^{\alpha} P\mathrm{H_2}^{\beta} \quad (2)$$

where *k* and *k`* follows an Arrhenius dependence with the temperature, [32,51,52] and α and β are the kinetic orders with respect ammonia and hydrogen, respectively.

The kinetic parameters were calculated by non-linear multivariable regression using Levenberg–Marquardt algorithm coupled to a Runge–Kutta–Fehlberg routine, using the steady-state ammonia mass balance in plug-flow reactor, [50]:

$$(-r_{NH3}) = \frac{dX_{NH_3}}{d(W_{cat}/F^0_{NH_3})} \quad (3)$$

X_{NH_3} is the ammonia conversion, W_{cat} / F^0_{NH3} is the spatial time (g_{cat} s/mol NH_3) and $(-r_{NH_3})$ is given by the power-law rate expression (2). The numerical solution of eqn (3), allows the calculation of the sum of the squared residuals (SSR), used as objective function minimized by the Levenberg–Marquardt algorithm:

$$SSR = \min \sum_{i=1}^{i=n} \left(X^{exp}_{NH_3} - X^{calc}_{NH_3}\right)^2 \quad (4)$$

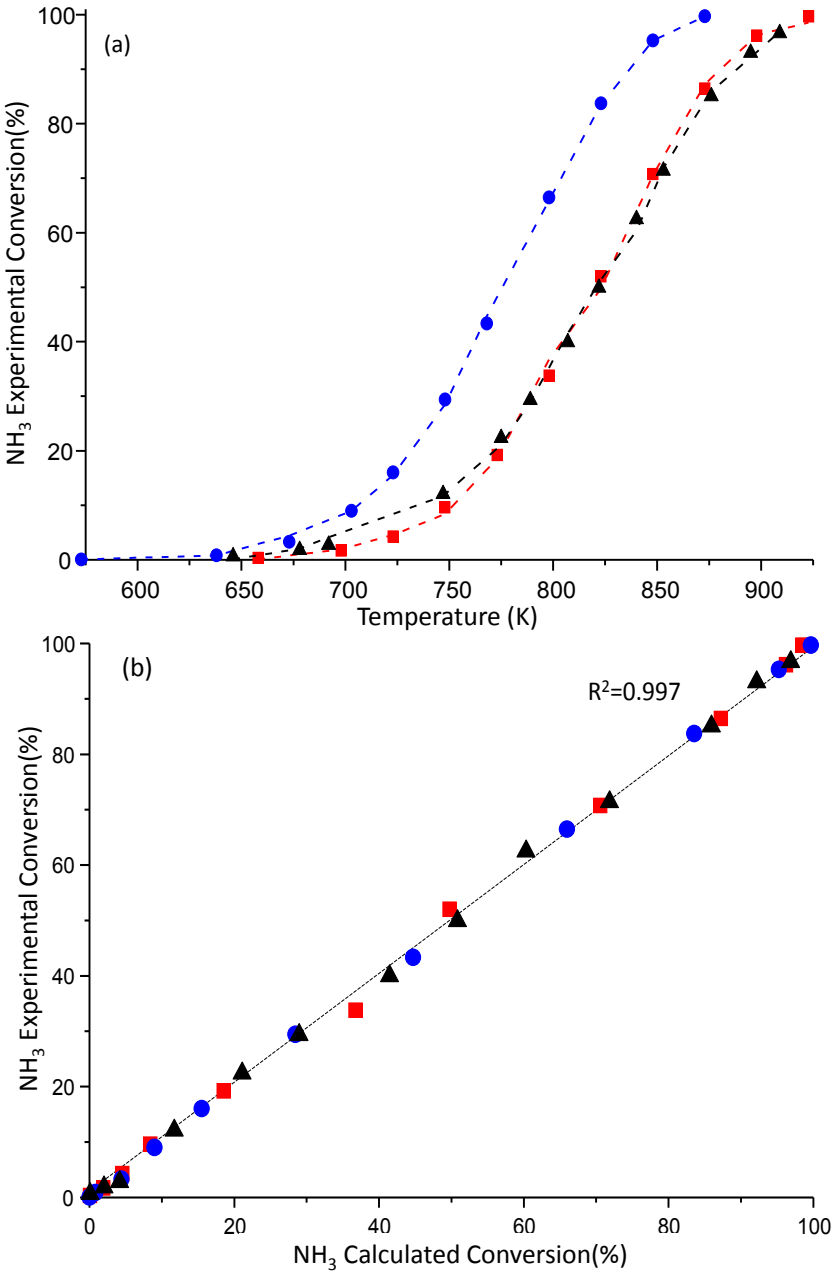

Fig. 6. (a) Dependence of NH3 conversion with reaction temperature (symbols: experimental data; dotted line: model simulation, eqn. 2) (●) Ru(NN)/Al/M; (■) Ru(Cl)/Al/M; (▲) Ru(acac)/Al/M; (b) Parity plot of the NH3 conversion data.

Fig.6 a-b, shows the results the experimental and model prediction of ammonia conversion vs. temperature data; and their excellent correlation in the parity plot (Fig. 6, b). As is in these figures the homoscedastic distribution of the errors along the entire range of conversions, indicates that power law model is an excellent approximation for the modelling of the experimental data and, according to the main hypothesis of the

306 Temkin-Pyzhev model, the rate determining step of the reaction mechanism is the
307 associative adsorption of N-adsorbed species.
308 In the Table 2 are shown the kinetic parameters of the Temkin-Pyzhev model. The low
309 values of the standard errors obtained in all the cases, indicate again the excellent fitting
310 achieved, and therefore the validity of the model. Thus, the valued of the apparent
311 activation energies presented in the Table 2 have the same tendency (i.e. Ru(NN)/Al/M
312 < Ru(Cl)/Al/M < Ru(acac)/Al/M) that the one obtaiend by direct aplication of the
313 Arrhenius equation to the low conversion data (Fig. 5). The good coincidence between
314 the results obtaiend using the diferential method of the low conversion data (Figure 5)
315 and the integral method of whole range of conversion data, eqn. 3 and Figure 6, if an
316 aditional proof of the confidence of the aproach used here.
317 Table 2: Kinetic parameters of Temkin-Pyzhev model.

Precursor Parameter	$Ru(NN)/Al_2O_3/M$ Value	$Ru(acac)/Al_2O_3/M$ Value	$Ru(Cl)/Al_2O_3/M$ Value
k (*)	6.99×10^{-04} ±error estandar	1.94×10^{-04} ±error estandar	1.04×10^{-02} ±
E(kJ/mol)	76.63±error estandar	154.81±error estandar	89.32±error estandar
α	0.72±error estandar	1.046±error estandar	0.781±error estandar
β	0.45±error estandar	-0.278±error estandar	0.439±error estandar
$-(\alpha/\beta)$	-1.57±error estandar	3.75±error estandar	-1.78±error estandar

318 * units: mol $NH_3 \cdot atm^{(\alpha+\beta)}/g_{cat} \cdot s$
319
320 According to the "Temkin formalism", the ratio α/β should be between 0.4 and 0.5,
321 however the result calculated by the fiting of the data on Figure 2 shows large
322 differences. In fact, the kinetic orders of ammonia and hydorgen show a great varibility
323 each other, which could be associated to the different catalyst intrinsinc nature, mainly
324 the average and distribution of particle sizez, the Ru content, and even the shape of the
325 particles, [33,53,54].

The lower activation energy and higher conversion of catalyst Ru(NN)/Al/M, compared to those prepared from the other precursors, can be attributed to its larger mean particle size (3.5 nm) which entails higher density of B_5-type sites. This behavior has been explained by compensatory effects [49,55], derived from the relationship between the activation energy of the rate-limiting step, and the stability of the reaction intermediates on the surface of the catalyst.

In spite of that the Temkin-Pyzhev model provide an reasonable acknowledge of the kinetic reaction mechanism, and a simple way to analyze the data, in some cases it is necesary to use a more robust model, which can predict the kinetic order evolutions during ammonia decomposition reaction. The kinetic orders and the apparent energies of activation shown in Table 2 are an average of all the individual values which could be calculated as the gas composition changes along the reactor length. In fact, we have previously demonstrated [50], that the variable kinetic orders and apparent activation energies frequently reported in the literature are consequence of misleading data analysis, and not a consequence of the any change in the controlling step of the reaction mechanism.

4. Conclusions

The results of this work show that the Ru catalyst in the form of honeycomb monoliths is a robust an active catalyst for H_2 generation form ammonia decomposition, thus being an enabling technology for the use of ammonia as practical H_2 storage media.

All the Ru-based catalysts used exhibited higher conversion in the decomposition of pure ammonia than Ni-based one, despite of ca. 5-fold larger metal loading of the latter.

Among all the Ru-based catalysts, the highest conversion and lowest apparent activation energy correspond to that prepared using ruthenium-nitrosyl-nitrate as precursor. This catalyst exhibited the largest mean particle size and the highest ratio of $Ru^0/Ru_{(total)}$ in

reduced state after the passivation step. Thus, the highest activity of Ru prepared from nitrosyl-nitrate could be explained by the higher proportion of B_5-type sites exposed, which have been related to particles with the same order of size.

The Temkin-Pyzhev (Power-Law) kinetic model provide an reasonable acknowledge of the reaction mechanism, and a simple way to analyze the data, in the whore range of ammonai conversions. The values of the kinetic orders, and the apparent energies of activation shown in Table 2, are valid to discriminate the intrisic differences observed between the catalysts, and to develop a complete model of the monolithic reactor.

Aknowledgements

The authors wants to aknowledge to the support of European Commission (FP7, Grant agreement nº 280658). Dr Armenise wants to aknowledge specially to University of Zaragoza, Institute of Carboquimica and Banco Santander Hispano to finance the doctoral fellow. Finnaly the authors wants to aknowledge to Universida Politecnica Salesiana to provide the economical support to attend the IMCCRE-2018.

References

[1] Mori D, Hirose K. Recent challenges of hydrogen storage technologies for fuel cell vehicles. Int J Hydrogen Energy 2009;34:4569–74. doi:http://dx.doi.org/10.1016/j.ijhydene.2008.07.115.

[2] Sakintuna B, Lamari-Darkrim F, Hirscher M. Metal hydride materials for solid hydrogen storage: A review. Int J Hydrogen Energy 2007;32:1121–40. doi:http://dx.doi.org/10.1016/j.ijhydene.2006.11.022.

[3] Schlapbach L, Zuttel A. Hydrogen-storage materials for mobile applications. Nature 2001;414:353–8.

[4] Holladay JD, Hu J, King DL, Wang Y. An overview of hydrogen production technologies. Catal Today 2009;139:244–60. doi:http://dx.doi.org/10.1016/j.cattod.2008.08.039.

[5] Cheng X, Shi Z, Glass N, Zhang L, Zhang J, Song D, et al. A review of PEM hydrogen fuel cell contamination: Impacts, mechanisms, and mitigation. J Power Sources 2007;165:739–56. doi:http://dx.doi.org/10.1016/j.jpowsour.2006.12.012.

[6] Dasireddy VDBC, Likozar B. COx-free hydrogen generation via decomposition of ammonia over copper and zinc-based catalysts. Fuel 2017;196:325–35. doi:https://doi.org/10.1016/j.fuel.2017.01.117.

[7] Schuth F, Palkovits R, Schlogl R, Su DS. Ammonia as a possible element in an energy infrastructure: catalysts for ammonia decomposition. Energy Environ Sci 2012;5:6278–89. doi:10.1039/C2EE02865D.

[8] Yin SF, Xu BQ, Zhou XP, Au CT. A mini-review on ammonia decomposition catalysts for on-site generation of hydrogen for fuel cell applications. Appl Catal A Gen 2004;277:1–9. doi:http://dx.doi.org/10.1016/j.apcata.2004.09.020.

[9] Ganley JC, Seebauer EG, Masel RI. Development of a microreactor for the production of hydrogen from ammonia. J Power Sources 2004;137:53–61. doi:http://dx.doi.org/10.1016/j.jpowsour.2004.05.032.

[10] Bradford MCJ, Fanning PE, Vannice MA. Kinetics of NH3Decomposition over Well Dispersed Ru. J Catal 1997;172:479–84. doi:http://dx.doi.org/10.1006/jcat.1997.1877.

[11] Pyrz W, Vijay R, Binz J, Lauterbach J, Buttrey DJ. Characterization of K-Promoted Ru Catalysts for Ammonia Decomposition Discovered Using High-Throughput Experimentation. Top Catal 2008;50:180–91. doi:10.1007/s11244-008-9095-y.

[12] Ju X, Liu L, Yu P, Guo J, Zhang X, He T, et al. Mesoporous Ru/MgO prepared by a deposition-precipitation method as highly active catalyst for producing COx-free hydrogen from ammonia decomposition. Appl Catal B Environ 2017;211:167–75. doi:https://doi.org/10.1016/j.apcatb.2017.04.043.

[13] Raróg-Pilecka W, Szmigiel D, Kowalczyk Z, Jodzis S, Zielinski J. Ammonia decomposition over the carbon-based ruthenium catalyst promoted with barium or cesium. J Catal 2003;218:465–9. doi:http://dx.doi.org/10.1016/S0021-9517(03)00058-7.

[14] Sørensen RZ, Klerke A, Quaade U, Jensen S, Hansen O, Christensen CH. Promoted Ru on high-surface area graphite for efficient miniaturized production of hydrogen from ammonia. Catal Letters 2006;112:77–81. doi:10.1007/s10562-006-0167-y.

[15] Armenise S, Roldán L, Marco Y, Monzón A, García-Bordejé E. Elucidation of Catalyst Support Effect for NH3 Decomposition Using Ru Nanoparticles on Nitrogen-Functionalized Carbon Nanofiber Monoliths. J Phys Chem C

2012;116:26385–95. doi:10.1021/jp308985x.
[16] Chen J, Zhu ZH, Wang S, Ma Q, Rudolph V, Lu GQ. Effects of nitrogen doping on the structure of carbon nanotubes (CNTs) and activity of Ru/CNTs in ammonia decomposition. Chem Eng J 2010;156:404–10. doi:http://dx.doi.org/10.1016/j.cej.2009.10.062.
[17] García-García FR, Álvarez-Rodríguez J, Rodríguez-Ramos I, Guerrero-Ruiz A. The use of carbon nanotubes with and without nitrogen doping as support for ruthenium catalysts in the ammonia decomposition reaction. Carbon N Y 2010;48:267–76. doi:http://dx.doi.org/10.1016/j.carbon.2009.09.015.
[18] Zheng W, Zhang J, Zhu B, Blume R, Zhang Y, Schlichte K, et al. Structure–Function Correlations for Ru/CNT in the Catalytic Decomposition of Ammonia. ChemSusChem 2010;3:226–30. doi:10.1002/cssc.200900217.
[19] Duan X, Qian G, Zhou X, Chen D, Yuan W. MCM-41 supported CoMo bimetallic catalysts for enhanced hydrogen production by ammonia decomposition. Chem Eng J 2012;207:103–8. doi:http://dx.doi.org/10.1016/j.cej.2012.05.100.
[20] Jacobsen CJH, Dahl S, Clausen BS, Bahn S, Logadottir A, Nørskov JK. Catalyst Design by Interpolation in the Periodic Table: Bimetallic Ammonia Synthesis Catalysts. J Am Chem Soc 2001;123:8404–5. doi:10.1021/ja010963d.
[21] Boisen A, Dahl S, Nørskov JK, Christensen CH. Why the optimal ammonia synthesis catalyst is not the optimal ammonia decomposition catalyst. J Catal 2005;230:309–12. doi:http://dx.doi.org/10.1016/j.jcat.2004.12.013.
[22] Czekajło Ł, Lendzion-Bieluń Z. Effect of preparation conditions and promoters on the structure and activity of the ammonia decomposition reaction catalyst based on nanocrystalline cobalt. Chem Eng J 2016;289:254–60. doi:http://dx.doi.org/10.1016/j.cej.2015.12.093.
[23] Srifa A, Okura K, Okanishi T, Muroyama H, Matsui T, Eguchi K. Hydrogen production by ammonia decomposition over Cs-modified Co3Mo3N catalysts. Appl Catal B Environ 2017;218:1–8. doi:https://doi.org/10.1016/j.apcatb.2017.06.034.
[24] Christian, Mitchell M, Kim D-P, Kenis PJA. Ceramic microreactors for on-site hydrogen production. J Catal 2006;241:235–42. doi:http://dx.doi.org/10.1016/j.jcat.2006.04.033.
[25] Deshmukh SR, Mhadeshwar AB, Vlachos DG. Microreactor Modeling for Hydrogen Production from Ammonia Decomposition on Ruthenium. Ind Eng Chem Res 2004;43:2986–99. doi:10.1021/ie030557y.
[26] Ganley JC, Thomas FS, Seebauer EG, Masel RI. A Priori Catalytic Activity Correlations: The Difficult Case of Hydrogen Production from Ammonia. Catal Letters 2004;96:117–22. doi:10.1023/B:CATL.0000030108.50691.d4.
[27] Plana C, Armenise S, Monzón A, García-Bordejé E. Ni on alumina-coated cordierite monoliths for in situ generation of CO-free H2 from ammonia. J Catal 2010;275:228–35. doi:http://dx.doi.org/10.1016/j.jcat.2010.07.026.
[28] Löffler DG, Schmidt LD. Kinetics of NH3 decomposition on polycrystalline Pt. J Catal 1976;41:440–54. doi:http://dx.doi.org/10.1016/0021-9517(76)90245-1.
[29] Vajo JJ, Tsai W, Weinberg WH. Steady-state decomposition of ammonia on the platinum(110)-(1 .times. 2) surface. J Phys Chem 1986;90:6531–5. doi:10.1021/j100282a023.
[30] Tsai W, Weinberg WH. Steady-state decomposition of ammonia on the ruthenium(001) surface. J Phys Chem 1987;91:5302–7. doi:10.1021/j100304a034.

[31] Kunsman CH. THE THERMAL DECOMPOSITION OF AMMONIA ON IRON CATALYSTS. II. J Am Chem Soc 1929;51:688–95. doi:10.1021/ja01378a005.
[32] Tamaru K. A “new” general mechanism of ammonia synthesis and decomposition on transition metals. Acc Chem Res 1988;21:88–94. doi:10.1021/ar00146a007.
[33] Chellappa AS, Fischer CM, Thomson WJ. Ammonia decomposition kinetics over Ni-Pt/Al2O3 for PEM fuel cell applications. Appl Catal A Gen 2002;227:231–40. doi:http://dx.doi.org/10.1016/S0926-860X(01)00941-3.
[34] Nishida T, Egawa C, Naito S, Tamaru K. Hydrogenation of nitric oxide on (0 0 1) and (1 1 10) surfaces of ruthenium. J Chem Soc{,} Faraday Trans 1 1984;80:1567–78. doi:10.1039/F19848001567.
[35] Djéga-Mariadassou G, Shin C-H, Bugli G. Tamaru’s model for ammonia decomposition over titanium oxynitride. J Mol Catal A Chem 1999;141:263–7. doi:http://dx.doi.org/10.1016/S1381-1169(98)00270-2.
[36] D’Souza L, Regalbuto JR, Miller JT. Preparation of carbon supported cobalt by electrostatic adsorption of [Co(NH3)6]Cl3. J Catal 2008;254:157–69. doi:http://dx.doi.org/10.1016/j.jcat.2007.12.007.
[37] Chan HYH, Takoudis CG, Weaver MJ. High-Pressure Oxidation of Ruthenium as Probed by Surface-Enhanced Raman and X-Ray Photoelectron Spectroscopies. J Catal 1997;172:336–45. doi:http://dx.doi.org/10.1006/jcat.1997.1841.
[38] Elmasides C, Kondarides DI, Grünert W, Verykios XE. XPS and FTIR Study of Ru/Al2O3 and Ru/TiO2 Catalysts: Reduction Characteristics and Interaction with a Methane−Oxygen Mixture. J Phys Chem B 1999;103:5227–39. doi:10.1021/jp9842291.
[39] Mazzieri V, Coloma-Pascual F, Arcoya A, L’Argentière PC, Fı́goli NS. XPS, FTIR and TPR characterization of Ru/Al2O3 catalysts. Appl Surf Sci 2003;210:222–30. doi:http://dx.doi.org/10.1016/S0169-4332(03)00146-6.
[40] Okal J, Zawadzki M, Tylus W. Microstructure characterization and propane oxidation over supported Ru nanoparticles synthesized by the microwave-polyol method. Appl Catal B Environ 2011;101:548–59. doi:http://dx.doi.org/10.1016/j.apcatb.2010.10.028.
[41] Rolison DR, Hagans PL, Swider KE, Long JW. Role of Hydrous Ruthenium Oxide in Pt−Ru Direct Methanol Fuel Cell Anode Electrocatalysts: The Importance of Mixed Electron/Proton Conductivity. Langmuir 1999;15:774–9. doi:10.1021/la9807863.
[42] Zhong Z, Aika K. Effect of ruthenium precursor on hydrogen-treated active carbon supported ruthenium catalysts for ammonia synthesis. Inorganica Chim Acta 1998;280:183–8. doi:http://dx.doi.org/10.1016/S0020-1693(98)00202-3.
[43] Maroto-Valiente A, Cerro-Alarcón M, Guerrero-Ruiz A, Rodríguez-Ramos I. Effect of the metal precursor on the surface site distribution of Al2O3-supported Ru catalysts: catalytic effects on the n-butane/H2 test. Appl Catal A Gen 2005;283:23–32. doi:http://dx.doi.org/10.1016/j.apcata.2004.12.047.
[44] Plana C, Armenise S, Monzón A, García-Bordejé E. Ni on alumina-coated cordierite monoliths for in situ generation of CO-free H2 from ammonia. J Catal 2010;275. doi:10.1016/j.jcat.2010.07.026.
[45] Jacobsen CJH, Dahl S, Hansen PL, Törnqvist E, Jensen L, Topsøe H, et al. Structure sensitivity of supported ruthenium catalysts for ammonia synthesis. J Mol Catal A Chem 2000;163:19–26. doi:http://dx.doi.org/10.1016/S1381-1169(00)00396-4.
[46] Choudhary T V, Sivadinarayana C, Goodman DW. Catalytic ammonia

517 decomposition: COx-free hydrogen production for fuel cell applications. Catal
518 Letters 2001;72:197–201. doi:10.1023/A:1009023825549.
519 [47] García-García FR, Guerrero-Ruiz A, Rodríguez-Ramos I. Role of B5-Type Sites
520 in Ru Catalysts used for the NH3 Decomposition Reaction. Top Catal
521 2009;52:758–64. doi:10.1007/s11244-009-9203-7.
522 [48] Karim AM, Prasad V, Mpourmpakis G, Lonergan WW, Frenkel AI, Chen JG, et
523 al. Correlating Particle Size and Shape of Supported Ru/γ-Al2O3 Catalysts with
524 NH3 Decomposition Activity. J Am Chem Soc 2009;131:12230–9.
525 doi:10.1021/ja902587k.
526 [49] Zheng W, Zhang J, Xu H, Li W. NH3 Decomposition Kinetics on Supported Ru
527 Clusters: Morphology and Particle Size Effect. Catal Letters 2007;119:311–8.
528 doi:10.1007/s10562-007-9237-z.
529 [50] Armenise S, García-Bordejé E, Valverde JL, Romeo E, Monzón A. A Langmuir-
530 Hinshelwood approach to the kinetic modelling of catalytic ammonia
531 decomposition in an integral reactor. Phys Chem Chem Phys 2013;15.
532 doi:10.1039/c3cp50715g.
533 [51] Emmett PH, Kummer JT. Kinetics of Ammonia Synthesis. Ind Eng Chem
534 1943;35:677–83. doi:10.1021/ie50402a012.
535 [52] M. Temkin VP. Kinetics of the synthesis of ammonia on promoted iron catalysts.
536 Acta Physicochim URSS, 1939;12:327–56.
537 [53] Bell TE, Torrente-Murciano L. H2 Production via Ammonia Decomposition
538 Using Non-Noble Metal Catalysts: A Review. Top Catal 2016;59:1438–57.
539 doi:10.1007/s11244-016-0653-4.
540 [54] Zhang J, Xu H, Li W. Kinetic study of NH3 decomposition over Ni
541 nanoparticles: The role of La promoter, structure sensitivity and compensation
542 effect. Appl Catal A Gen 2005;296:257–67.
543 doi:https://doi.org/10.1016/j.apcata.2005.08.046.
544 [55] Bligaard T, Honkala K, Logadottir A, Nørskov JK, Dahl S, Jacobsen CJH. On the
545 Compensation Effect in Heterogeneous Catalysis. J Phys Chem B
546 2003;107:9325–31. doi:10.1021/jp034447g.
547